UCRL-53882

A Centered Artificial Viscosity for Cells with Large Aspect Ratio

L. G. Margolin

August 15, 1988

Lawrence Livermore National Laboratory

Work performed under the auspices of the U.S. Department of Energy by Lawrence Livermore National Laboratory under Contract W-7405-ENG-48.

UCRL-53882
Distribution Category UC-705

A Centered Artificial Viscosity for Cells with Large Aspect Ratio

L. G. Margolin

Manuscript date: August 15, 1988

LAWRENCE LIVERMORE NATIONAL LABORATORY
University of California • Livermore, California • 94550

Available from: National Technical Information Service • U.S. Department of Commerce
5285 Port Royal Road • Springfield, VA 22161 • A02 • (Microfiche A01)

Contents

A Centered Artificial Viscosity for Cells with Large Aspect Ratio

L. G. Margolin

Abstract

I have developed a new artificial viscosity for numerical fluid dynamics codes in two dimensions. The formulation combines the advantages of a cell-centered treatment with the ability of the edge-centered method to handle cells with large aspect ratio. This report describes the derivation of the new viscosity, whose magnitude and tensor properties both differ from standard treatments. The new viscosity has been implemented in the SHALE code. I present calculations on two variations of a test problem representing a shock propagating obliquely through a two-dimensional mesh.

I. Introduction

In 1950 von Neumann and Richtmyer [1] introduced the idea of an artificial viscosity to numerically calculate fluid flows with shocks. Artificial viscosity, by analogy with physical viscosity, smears a shock discontinuity in space without affecting the Hugoniot conditions across the shock. It is found experimentally that when the shock is spread over about three or four cell lengths, the numerical state behind the shock can approximate the physical solution with few or no unphysical oscillations.

The von Neumann-Richtmyer viscosity was designed for one-dimensional flows. The viscous stress is represented as a scalar pressure, and is calculated at the same place as the physical pressure—i.e., at the cell center. The viscous stress has the form

$$q = \lambda \frac{\partial u}{\partial x} \tag{1}$$

where λ is the coefficient of artificial viscosity. Dimensionally, λ consists of a density, a velocity, and a length scale. The velocity is usually chosen to be a combination of a local sound speed and the change in material velocity across the cell [2]. The density is the current cell density, and the length is the width of the cell.

Generalizing Eq. (1) for two- and three-dimensional calculations introduces some new choices and difficulties. With respect to the velocity gradient, there are two possibilities that determine the tensor character of the viscosity. Fluid codes replace the velocity gradient with the divergence of the velocity, and so create a scalar viscous pressure. Solid mechanics codes use the full velocity gradient tensor—sometimes called the strain-rate tensor—and create a tensor viscous stress [2]. The original version of SHALE [3] was written to allow the user to choose an arbitrary combination of these two viscosities.

A more difficult decision is how to choose the length scale. In many problems, quadrilateral cells have very different sizes for adjacent edges—i.e., have large aspect ratio. Shocks do not always propagate perpendicular to one set of cell edges or the other, and in Lagrangian calculations, the mesh may become totally irregular. The underlying idea that should be preserved is to smear the shock over about three cells in the direction of propagation of the shock. Wilkins [2] uses the local accelerations to define the shock direction, and then describes a method to find the length scale of the cell in that

direction. SHALE [3] uses a similar method based on the direction of the local velocity field. Such schemes work well so long as the aspect ratio of the cells is not too large. In SHALE, as the aspect ratio approaches about 10:1, difficulties arise.

At Livermore, problems frequently arise in which it is desired to use cells with aspect ratios of several hundred to one and more. Bill Schulz [4] developed a variant of the staggered mesh scheme in which the artificial viscosity is calculated at the cell edges rather than the cell centers. Effectively, each side of the cell is like a "spring" whose spring constant is chosen appropriately for its length. Schulz' hydro was, and still is, very successful.

Another very different method for simulating flows with shocks was first proposed by Godunov [5] nearly 30 years ago. The Godunov schemes do not solve the fluid equations directly. Instead, they approximate the solution of a complex problem as the superposition of many solutions to much simpler problems. The Godunov schemes as first proposed were very diffusive. Also, even the simpler problems—Riemann problems—were only easily solved for a few analytic equations of state. About 10 years ago, two advances revived the interest in Godunov schemes. The first advance involved using higher-order spatial approximations and monotonicity constraints in defining the Riemann problems [6]. The second advance was in the construction of fast, approximate Riemann solvers for more general (and even tabular) equations of state [7].

An interesting feature of the Godunov schemes is that they do not require the addition of an explicit artificial viscosity. The extra diffusion necessary for any numerical scheme to represent shocks is added implicitly in the form of truncation error in the Riemann solution. Although the use of an explicit artificial viscosity has made it possible to calculate flows with shocks, it must be admitted that its use creates a whole new set of problems [8,9]. The new Godunov schemes appear to add a minimal amount of diffusion. To emphasize this point, Colella and Saltzman [10] compared their Lagrangian Gudonov code with a traditional explicit viscosity code on a test problem that generates a shock moving obliquely to a mesh.

In fact, the comparison pointed up some severe problems in the implementation of the edge-centered viscosity. These were traced to the tensor character of the viscosity and were repaired by a rather simple change that is attributed to R. Barton and is described in Appendix B. The published version of SHALE, with its cell-centered viscosity, had no trouble running the test problem, which is commonly called the Saltzman piston problem, and I have included some of these results in Appendix A.

The cells in the Saltzman piston problem have approximately a 1:1 aspect ratio. I made a simple change by increasing the width of the piston face while keeping the problem length constant. The widening is perpendicular to the direction of flow, and one might expect this simple change would not alter the code results at all. In fact, most codes based on Schulz' edge-centered viscosity showed a small improvement. However, SHALE results degenerated and for an aspect ratio of 100:1 were quite poor.

The problem was found to lie on the boundaries where jets formed. The boundary cells deformed with the segment of the cell lying on the boundary getting much shorter than parallel sides on interior cells. The short length controlled the timestep. The proper approach appeared to be imitating the Schulz viscosity with at least two length scales for each cell. Implementing the edge-centered viscosity in SHALE would have required considerable rewriting of the code. However, I found a simpler solution. I derived a cell-centered viscosity that produced the same forces between the adjacent nodes, taken two at a time, as the edge-centered viscosity. In addition, it was possible to preserve most of the advantages of the cell-centered formulation.

After this introduction, it is possible to summarize the rest of this paper. In the next section, I will give a brief description of Schulz' tensor viscosity. I will also describe some of the details of how SHALE uses its cell-centered viscosity. In Sec. III, I will derive a cell-centered formalism that reproduces the forces of an edge-centered viscosity. In this section I will also show some results from the standard test problem. In Secs. IV and V, I will turn attention to the test problem with large aspect ratio cells. Although SHALE will now run this problem, the results exhibit a small jet of fluid along the axis of symmetry. I will present a discussion of this phenomenon, which is also seen in codes with edge-centered viscosity, and suggest several improvements to Schulz' treatment that eliminate the jet. In Appendix A, I will describe the test problem in some detail, and show results from SHALE using the old viscous treatment. Finally, in Appendix B I will describe Barton's improvement to Schulz' viscosity.

II. Some Details of Artificial Viscosity Formulations

In this section I will describe a simplified version of an edge-centered viscosity. I have tried to distill from Schulz' work the most important ideas while ignoring the details of the implementation. A much more detailed account of Schulz' work can be found in his article [4]. I have also chosen different notation from Schulz, partly to emphasize the true tensor nature of the viscosity and partly to be consistent with the notation used by SHALE.

The notation is illustrated graphically in Fig. 1. SHALE uses general quadrilateral cells whose vertices are numbered counter-clockwise. It is not important which vertex is labeled as number 1. The coordinates of vertex 1, which happens to be the lower right vertex in Fig. 1, has coordinates (x_1,y_1), etc. With respect to Fig. 1, one can define several sets of vectors. First, the vector that joins vertex 1 to vertex 2 is

$$\Delta\mathbf{X}^{12} = (x_2 - x_1, y_2 - y_1) \tag{2}$$

and similarly for the other four sides – $\Delta\mathbf{X}^{23}$, $\Delta\mathbf{X}^{34}$, and $\Delta\mathbf{X}^{41}$. Second, the vector $\mathbf{Y}^{12}$ is perpendicular to the side $\Delta\mathbf{X}^{12}$, points out of the cell, and has the same magnitude as the length of the side.

$$\mathbf{Y}^{12} = (y_2 - y_1, x_1 - x_2) \tag{3}$$

There are three more of these vectors also, each associated with a side of the cell—$\mathbf{Y}^{23}$, $\mathbf{Y}^{34}$, and $\mathbf{Y}^{41}$.

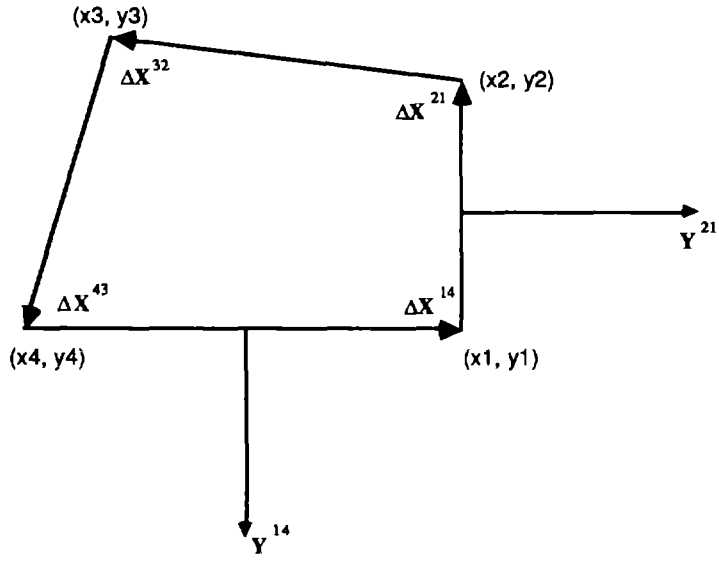

Figure 1. A typical quadrilateral cell in SHALE. Vertices are numbered counter-clockwise from the lower right corner. The coordinates associated with each vertex are shown in parenthesis. The cell edges are vectors—for example, the vector $\Delta\mathbf{X}^{14}$ extends from vertex 4 to vertex 1. Each edge has an associated vector, Y, perpendicular to the edge and pointing out of the cell. For example, the vector $\mathbf{Y}^{14}$ is associated with the edge $\Delta\mathbf{X}^{14}$. The opposite sides of the quadrilateral are not necessarily parallel to each other.

It is convenient to define another set of four vectors

$$\begin{aligned} \mathbf{k} &= 0.5\,(\Delta X^{12} - \Delta X^{34}) \\ \mathbf{l} &= 0.5\,(\Delta X^{23} - \Delta X^{41}) \\ \mathbf{m} &= 0.5\,(Y^{12} - Y^{34}) \\ \mathbf{n} &= 0.5\,(Y^{23} - Y^{41}) \end{aligned} \tag{4}$$

When the opposite sides of the quadrilateral cell are parallel, then **k** is parallel to the side joining vertex 1 to vertex 2, and also the side joining vertex 3 to vertex 4. The most general cell does not have its opposite sides parallel, and then k has the average direction of these pairs of opposite sides. Note that

$$\mathbf{m} \cdot \mathbf{k} = \mathbf{n} \cdot \mathbf{l} = 0$$

Along each side, there is also a relative velocity $\Delta\mathbf{u}$. For example, the relative velocity between vertex 1 and vertex 2 is

$$\Delta u^{21} = (u_2 - u_1, v_2 - v_1) \tag{5}$$

The cell density is ρ and the specific internal energy is I. These are calculated at the cell center. In SHALE, the coordinates of the cell center are just the average coordinates of the four vertices.

Schulz defines a viscous stress $q_{\alpha\beta}$ along the edge ΔX^{21}. In the simplest analogy to the von Neumann-Richtmyer viscosity, the stress has a magnitude equal to $\rho\,(\Delta u^{21})^2$ whenever Δu^{21} causes the edge to decrease in length, and zero otherwise. It is applied to an length like $|Y^{21}|$ and produces a force between node 1 and node 2. The force has the same direction as ΔX^{21}—e.g., the force pushes the nodes apart along the line that joins them.

(In fact, this description is not quite correct. Schulz' viscosity is not a true tensor. Its magnitude contains a second derivative of Δu so that it vanishes during uniform compression. Further, the area it applies to is an average over the lengths of the two adjacent sides. Schulz' averaging process is complex and has changed several times over the years.)

An important modification to this viscosity concerning its tensor character was suggested by Bob Barton. Barton realized that the resultant force between the nodes should be in the direction of the relative velocity itself, $\Delta\mathbf{u}$, rather than along the edge. This change greatly improves the performance of edge-centered codes on the Saltzman test problem. Some results are shown in Appendix B.

SHALE uses an artificial viscous stress tensor calculated at the center of the cell. The form of the viscosity is

$$q_{\alpha\beta} = \frac{\lambda\mu}{2}\left[\frac{\partial u_\alpha}{\partial x_\beta} + \frac{\partial u_\beta}{\partial x_\alpha}\right] + \lambda\,(1-\mu)\,\frac{\partial u_\gamma}{\partial x_\gamma}\,\delta_{\alpha\beta} \tag{6}$$

Here α and β are tensor indices in space, and are not related to the logical coordinates of a cell. $\delta_{\alpha\beta}$ is the Kronecker delta, equal to one when $\alpha = \beta$ and zero otherwise. Summation is implied over repeated indices. The coefficient of artificial viscosity, λ, is defined

$$\lambda = \rho\,(c_1\,c_s\,l - c_q\,D\,l^2)$$

where

l is a characteristic mesh length of the cell

c_s is a characteristic sound speed

c_l and c_q are dimensionless numbers of order 1

D is the divergence of the velocity field

The input number μ is the fraction of the viscosity that is a tensor, and $(1 - \mu)$ is the fraction that is scalar.

In Fig. 2, I show a vertex surrounded by four cells, which are again numbered counter-clockwise. The dotted lines joining the cell centers form a control volume, which is an eight-sided figure used to accelerate the node. Newton's law says that the acceleration of the center of mass of this control volume is surface integral of the stress over the control volume divided by its mass. The surface integral is evaluated by assuming that the stress is piecewise constant within each cell.

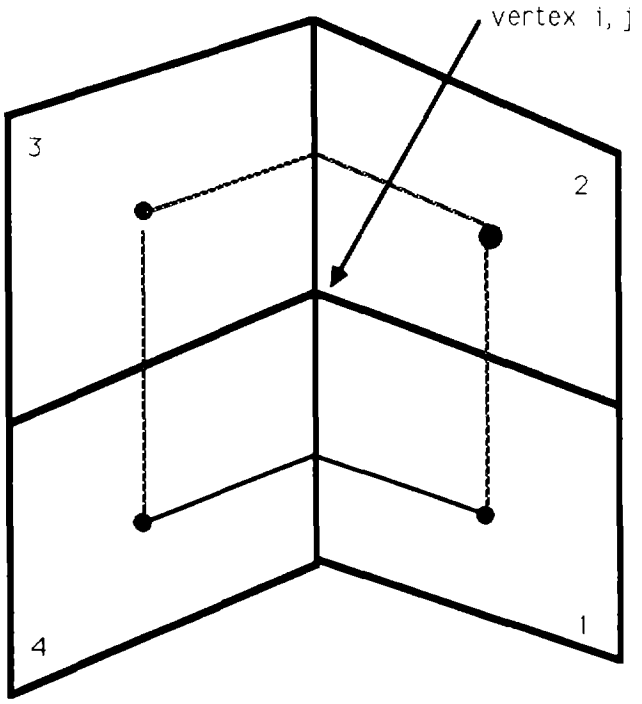

Figure 2. The pressures in the four cells surrounding the vertex i,j are used to compute the acceleration at the vertex. The eight-sided figure that surrounds the vertex is formed by joining the cell center of each cell to the centers of the cell edges that contain vertex i,j and is named the momentum control volume. The surface integral of the stresses is a force that, by Newton's law, accelerates the center of mass of the momentum control volume. This surface integral is approximated by a sum, assuming that the stress is piecewise constant in each of the four cells surrounding the vertex.

Returning now to Fig. 1, the cell stress $q_{\alpha\beta}$ produces forces that contribute to the acceleration of each of the four vertices that define the cell. These forces can be written

$$
\begin{aligned}
F_\alpha \text{ (vertex 1)} &= 0.5 * q_{\alpha\beta} (+ Y^{41} + Y^{12}) \\
F_\alpha \text{ (vertex 2)} &= 0.5 * q_{\alpha\beta} (+ Y^{12} + Y^{23}) \\
F_\alpha \text{ (vertex 3)} &= 0.5 * q_{\alpha\beta} (+ Y^{23} + Y^{34}) \\
F_\alpha \text{ (vertex 4)} &= 0.5 * q_{\alpha\beta} (+ Y^{34} + Y^{41})
\end{aligned}
\tag{7}
$$

III. The New Viscosity

In the previous section, I described the forces generated by an edge viscosity. I also described how SHALE uses its centered viscosity to generate forces on the nodes. Now, I will combine these ideas to formulate a centered viscosity that produces almost the same forces between the nodes as does the edge viscosity.

A small qualification is necessary because the edge viscosity is able to produce four different forces in a cell—i.e., one for each edge. The centered viscosity can produce only two distinct forces. The extra forces in the edge viscosity are possible essentially because one sacrifices the tensor character of the viscous tensor. To see that the centered viscosity allows only two forces, consider again the cell of Fig.1. Referring to Eq. (7), one sees that the relative force between nodes 1 and 2 is exactly the relative force between nodes 3 and 4. That is,

$$
\begin{aligned}
\Delta F^{12} &= -q_{\alpha\beta} n_\beta = \Delta F^{43} \\
\Delta F^{23} &= -q_{\alpha\beta} m_\beta = \Delta F^{14}
\end{aligned}
\tag{8}
$$

However, the edge viscosity will produce different forces on these edges unless $\Delta u^{21} = \Delta u^{34}$. This condition is

$$
\begin{aligned}
u_1 - u_2 + u_3 - u_4 &= 0 \\
v_1 - v_2 + v_3 - v_4 &= 0
\end{aligned}
\tag{9}
$$

The condition expressed by Eq. (9) means that the two viscous treatments can only be equivalent if the velocity field has no hourglassing. If there is an hourglassing component, then the centered viscosity will produce no forces to damp it. However, SHALE has other, more effective ways to suppress hourglassing. In a previous paper [11] I showed that the hourglassing represents unphysical deformation modes. Rather than use artificial viscous forces to damp these modes, SHALE uses projection operators to selectively identify and filter them.

To proceed, then, I will assume that the conditions of Eq. (9) hold. This does not mean that the theory will not apply when hourglassing is present. Rather, I shall simply ignore that part of the velocity that corresponds to the hourglassing component whenever it is present. The simplest way to accomplish this is to define the relative velocities along the edges in terms of the spatial gradients of velocity in the cell, rather than as the difference of actual velocities of the nodes. This is equivalent to filtering the velocity field as described in [11].

The relative velocities can be defined in terms of the spatial gradients (an appropriate differencing for the spatial derivatives of velocity can be found in [12]):

$$\Delta u^{21} = \frac{\partial u_\alpha}{\partial x_\beta} k_\beta = A_\alpha$$

$$\Delta u^{32} = \frac{\partial u_\alpha}{\partial x_\beta} l_\beta = B_\alpha \tag{10}$$

Now if the cell-centered viscous stress $q_{\alpha\beta}$ is to produce the same internodal forces as Schulz' edge viscosity, then it must satisfy the following two equations:

$$q_{\alpha\beta} m_\beta = C^1 \frac{\partial u_\alpha}{\partial x_\beta} k_\beta = C^1 A_\alpha \tag{11}$$

$$q_{\alpha\beta} n_\beta = C^2 \frac{\partial u_\alpha}{\partial x_\beta} l_\beta = C^2 B_\alpha \tag{12}$$

These equations guarantee that the centered viscous forces will be in the correct direction. Proper choice of the two coefficients C^1 and C^2 then guarantees the desired magnitudes. A solution can be easily written down.

$$q_{\alpha\beta} = C^1 \frac{A_\alpha k_\beta}{|k|} + C^2 \frac{B_\alpha 1_\beta}{|1|} \tag{13}$$

(To verify that this is a solution, recall that $\mathbf{m} \cdot \mathbf{k} = \mathbf{n} \cdot \mathbf{l} = 0$.)

Next, consider the coefficients C^1 and C^2 in more detail. These are scalars, and continuing to follow Schulz, should contain the term $\rho(\Delta u)^2$. This means that C^1 should contain $|\mathbf{A}|$, and C^2 should contain $|\mathbf{B}|$. To more closely approximate the previous viscous treatment in SHALE [see Eq. (3)], I also add a linear term proportional to the local sound speed, c_s. This term helps damp the longer wavelength oscillations behind a shock. It is also important for weaker waves, especially elastic waves in solids.

I also want to preserve the idea of a one-sided viscosity—i.e., one that only turns on in compression. In the Schulz formulation the viscosity is on whenever the relative velocity causes the nodes to get closer: that is, for nodes 1 and 2 whenever

$$\mathbf{A} \cdot \mathbf{k} < 0 \tag{14}$$

There are problems with this strategy. Figures 3a and 3b show a large shear, nearly perpendicular to one cell edge. In Fig. 3a, the switch defined by Eq. (14) is on, resulting in a large viscosity. In Fig. 3b, the cell edge is slightly altered, causing the switch to be off and resulting in no viscosity. I would like to avoid this sensitivity to the orientation of the cell side behavior, and would prefer a switch that senses the presence of a shock independent of the cell orientation. The old version of SHALE used the sign of the divergence of the velocity field as a switch and this seems to have the right properties. Thus, define the switch

$$s = 0.5\left[1 - \frac{d}{|d|}\right] \quad \text{where} \quad d = \frac{\partial u_\gamma}{\partial x_\gamma} \tag{15}$$

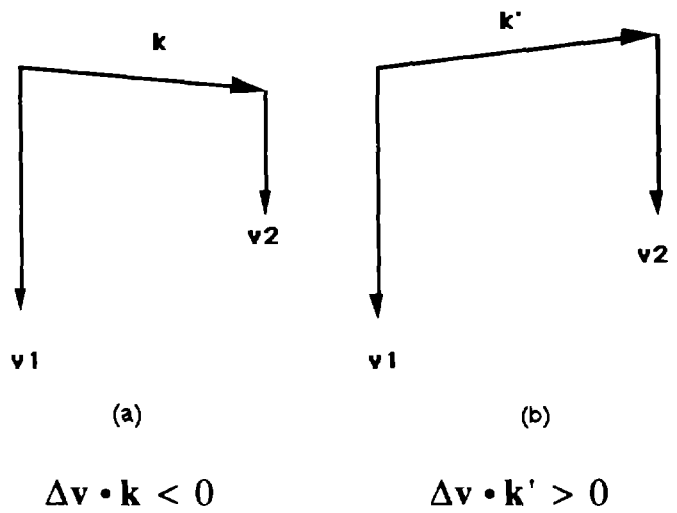

Figure 3. A small change in the orientation of the cell side k changes the switch from on to off for this shear flow.

Finally, then, the coefficients of viscosity are defined by

$$C^1 = \rho\left[\, c_1 c_s - c_q \,|\, \mathbf{A} \,|\,\right] s$$

$$C^2 = \rho\left[\, c_1 c_s - c_q \,|\, \mathbf{B} \,|\,\right] s \qquad (16)$$

where c_s is the sound speed calculated at the center of the zone.

The constants c_1 and c_q are dimensionless numbers that are chosen to yield the sharpest possible shock that does not produce spurious oscillations behind the shock. In SHALE, both these constants seem to be optimally chosen equal to 1. The form of the coefficients in Eq. (16) seems somewhat arbitrary, since the values $|\mathbf{A}|$ and $|\mathbf{B}|$ still depend on the orientation of the cell. In the next section, I will return to this point and show that these coefficients should really be related to the Courant condition that controls the timestep. However, for cells with approximately 1:1 aspect ratio, the viscosity described above is quite satisfactory.

Before showing some results, there is one more point to mention. Referring back to Eq. (13), it is clear that the viscous tensor is not necessarily symmetric. Schulz also recognized this point and in his article [4] points this out as an inadequacy of his formulation. This problem (if it is a problem) is easily overcome in the cell-centered formulation by the simple expedient of symmetrizing the tensor. On theoretical grounds, one would expect the nonsymmetric formulation to be superior. For one thing, the symmetrized tensor leads to mode conversion; that is, a shear flow in which the velocities are all parallel will lead to viscous forces that cause acceleration in the perpendicular direction. Also, the nonsymmetric viscosity can be shown to be always dissipative—its work is always positive whereas the symmetrized form does not have this property. However, running both forms on SHALE showed that the symmetrized form worked better. In fact, the nonsymmetric form does yield better results, but only when the appropriate boundary conditions are implemented. I will postpone this discussion to Sec. IV and note that the results presented next used the symmetrized viscosity.

The results of a SHALE run on the Saltzman piston problem are shown in Fig. 4 where the mesh is plotted at the standard time (t = 0.375; see Appendix A), and in Fig. 5 where the density contours are overlaid on the mesh. A full description of the Saltzman piston problem is found in Appendix A. Note that the plots are shown in a left-handed coordinate system where the positive x-direction is 90°

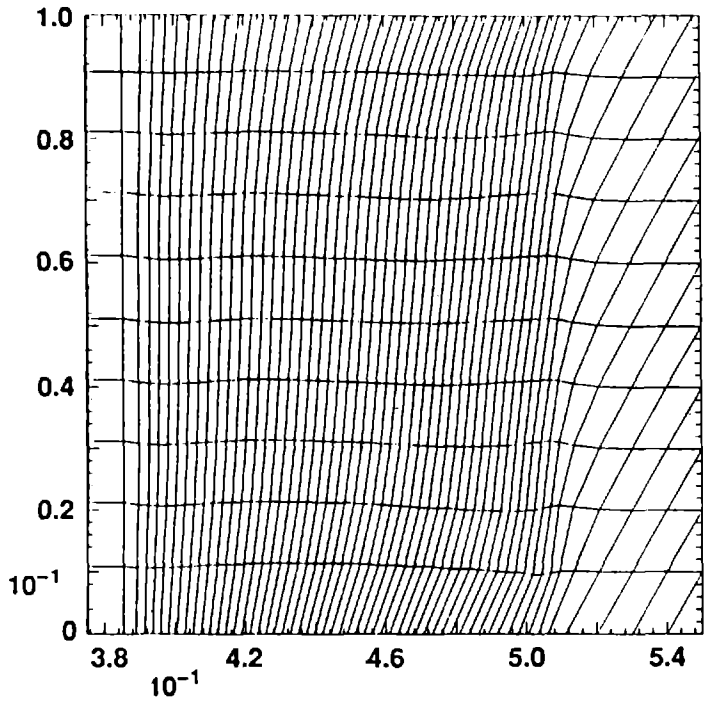

Figure 4. The Saltzman piston problem, showing the mesh at the standard time. The shock is halfway down the original mesh. This calculation used the symmetrized viscous stress tensor.

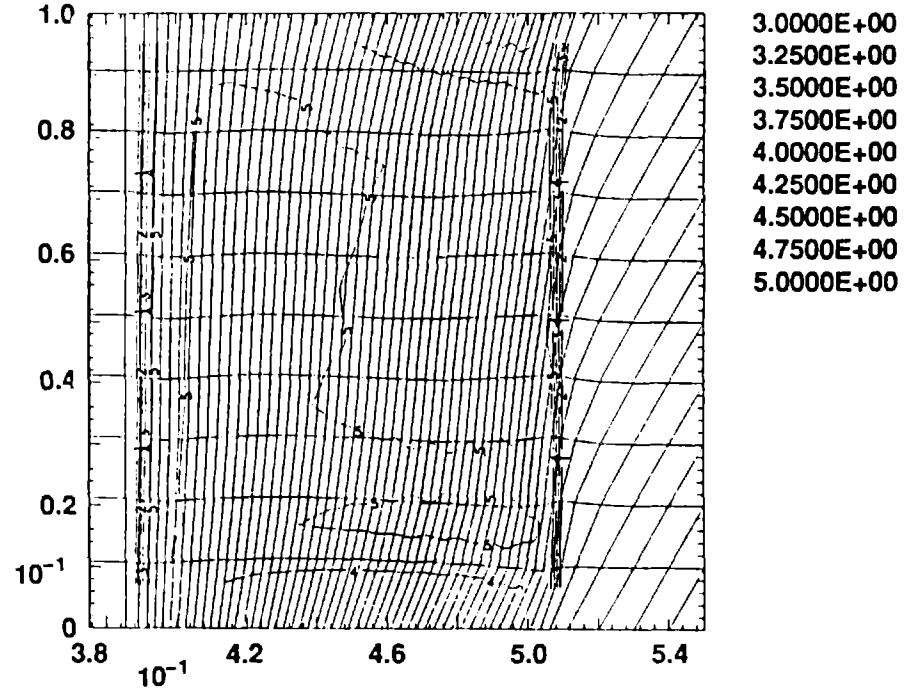

Figure 5. The same calculation as shown in Fig. 4, with contours of density superposed on the mesh.

counter-clockwise of the positive y-direction. The shock is halfway down the mesh. The density behind the shock is almost always within 5% of the correct value. The contours at the piston face are an effect known as wall-heating and result from the impulsive start of the problem. There is a small effect on the top and bottom sides of the cylinder, which I have traced to the way the area factors are defined. Even though the velocity field should only have a nonzero component along the y-axis (along the cylindrical axis), SHALE sees the pressure as having small gradients along the x direction (normal to the cylindrical axis). These gradients cause small waves to propagate across the cylinder; the slight waviness of the horizontal mesh lines are also due to this effect.

These results are qualitatively similar to the results generated by the old viscous treatment in SHALE, and shown in Appendix A. The contours in the new treatment are somewhat cleaner. The biggest difference is that the new SHALE runs about 15% faster than the old, mainly because the internode spacing on the bottom horizontal boundary (which controls the timestep) remains more uniform. However, the new viscosity was not expected to be much different than the old when the mesh consists of cells with aspect ratio of about 1:1.

IV. Boundary Conditions

To further test the new viscosity, I modified the Saltzman problem by stretching the cells—i.e., widening the piston face by a factor of 100 while leaving the length of the cylinder unchanged. The SHALE calculation failed almost immediately in the following sequence of steps. SHALE calculated a negative work contribution from the viscous stresses that led to a net negative internal energy. Shortly afterward, the code tried to calculate the sound speed in that cell, and stopped after trying to take the square root of a negative number.

Negative internal energies occur in Schulz' hydro also. The usual fix is to either set any negative viscous work to zero, or to simply ignore any viscous stress tensor that leads to a negative work increment (i.e., set both the work and the viscous stresses to zero). Neither of these fixes seems justifiable to me, for they address a symptom rather than the problem itself.

In SHALE, the problem is that the symmetrized viscosity can convert internal energy into kinetic energy. In particular, the presence of a shear flow in one direction can create a shear flow in the perpendicular direction. A shear velocity field and the direction of the resultant forces produced by the symmetrized viscous tensor are shown in Fig. 6a. The symmetrized viscosity tensor cannot change the angular velocity associated with the cell, and so must produce horizontal forces in addition to the vertical forces that reduce the relative velocity along the edges. The original nonsymmetric viscosity was constructed *a priori* to produce only those forces that exactly oppose the relative velocity along each edge, as shown in Fig. 6b.

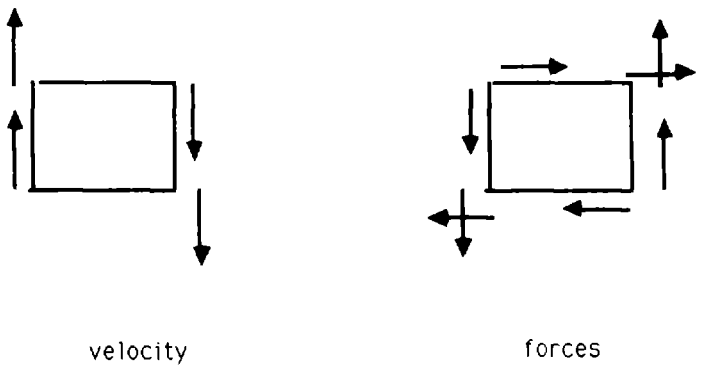

Figure 6a. A shear velocity field and the forces produced by the symmetrized viscous tensor.

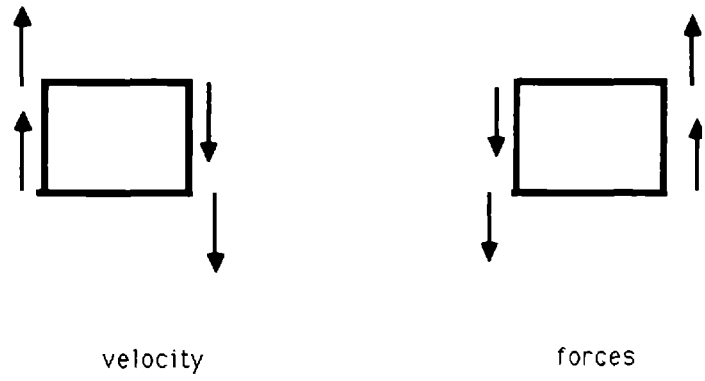

Figure 6b. The forces produced by the nonsymmetric viscosity are constructed to exactly oppose the relative velocity along the edge.

The total viscous work is the sum of several terms. The negative work associated with these shear terms dominates the total work in the 100:1 aspect ratio problem, but not in the 1:1 problem. Nevertheless, even in the 1:1 problem, some of the viscous forces are converting internal energy to kinetic energy and are not dissipative.

Mathematically, the work done by any symmetric stress tensor $\sigma_{\alpha\beta}$ leads to a change in internal energy (I)

$$\frac{dI}{dt} = \frac{\sigma_{\alpha\beta}\,\dot{\varepsilon}_{\alpha\beta}}{\rho} \tag{17}$$

where the rate of strain tensor is given by

$$\dot{\varepsilon}_{\alpha\beta} = \frac{1}{2}\left[\frac{\partial u_\alpha}{\partial x_\beta} + \frac{\partial u_\beta}{\partial x_\alpha}\right]$$

When the stress tensor is nonsymmetric, the additional work due to changing the angular velocity must be added. For the nonsymmetric stress tensor $q_{\alpha\beta}$, the change in internal energy is

$$\frac{dI}{dt} = \frac{q_{\alpha\beta}}{\rho}\,\frac{\partial u_\alpha}{\partial x_\beta} \tag{18}$$

Now when the nonsymmetric viscous stress of Eq. (13) is substituted into Eq. (18), the change in internal energy is proportional to the squares of the magnitudes of the vectors **A** and **B**, and is nonnegative. However, when this stress is symmetrized and substituted into Eq. (17), the change in internal energy can be negative. This is a consequence of the specific form of the viscosity, for the symmetric viscous tensor in SHALE's old formulation, Eq. (6), does lead to a nonnegative change of internal energy.

The previous arguments led me to conclude that the nonsymmetrized viscous tensor is superior. However, when I implemented it in SHALE even in the 1:1 aspect ratio problem, the results were inferior to the symmetrized tensor. It turns out that the problem lies in the form of the boundary conditions that are used. The horizontal boundaries, perpendicular to the piston face and parallel to the main direction of flow, are free slip. This means that the nodes on these boundaries are constrained to move horizontally. In SHALE (and most other codes), free slip boundaries are implemented by assuming a ghost cell on the other side of the boundary that is the mirror image of the true boundary cell, both in its geometry and in its velocities. The resultant forces guarantee that the acceleration is

parallel to the boundary. However, these reflection boundaries also affect the tangential accelerations that are calculated for the boundary nodes.

There is no particular reason to make this specific choice about the tangential accelerations, and there is at least one other choice. One could simply extrapolate the boundary cell to construct the ghost cell. These two boundary conditions are shown in Fig. 7. (However, in cylindrical coordinates, there is a physical reason to prefer the reflected symmetry along the axis of symmetry.)

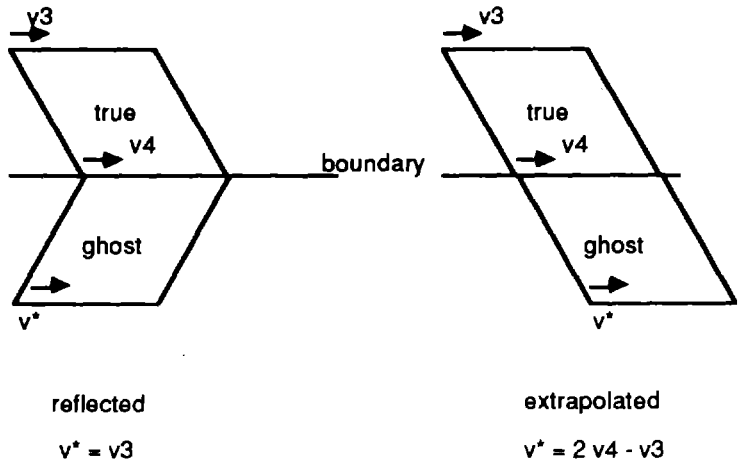

Figure 7. Two possible ways to formulate boundary conditions for free slip boundaries.

Having the geometry and the velocities, it is easy to construct the viscous tensor for the two possible ghost cells shown in Fig. 7. The only difference has to do with the stress component q^*_{yx}:

$$q^*_{yx} = -q_{yx} \quad \text{reflected boundary}$$
$$q^*_{yx} = q_{yx} \quad \text{extrapolated boundary} \tag{19}$$

Here, the q^* refers to the ghost cell and q to the true cell. The reader is reminded that y is the horizontal axis in Fig. 7.

The meaning of Eq. (19) is this. When the forces on the nodes 1 and 4 of the true cell in Fig. 7 are computed, the reflected boundary nodes see forces due to the yx-component. The extrapolated boundary nodes see no net forces—the forces produced by the true and the ghost cells cancel. This is an easy boundary condition to implement. The results are shown in Figs. 8 and 9 for the 1:1 aspect ratio problem. When compared with the results of the symmetrized viscous tensor, the main differences are found in the boundary cells. Since the logical j-lines (the mostly vertical lines of the mesh) are initially straight lines, and move with the local material velocity, these lines should remain straight after the shock has passed. The calculation with the symmetrized viscosity shows large bends occurring for the sides of the cells on the boundaries, whereas the calculation with the nonsymmetrized viscosity keeps the j-lines much straighter. The contours of density for the two calculations are very similar, and the average computational timestep associated with the nonsymmetrized viscosity is a few per cent larger.

The main conclusion of this section is that the nonsymmetric viscous tensor, with extrapolated boundary conditions, is as good or slightly better than the symmetrized viscosity on the 1:1 aspect ratio piston problem. In addition, it guarantees that the viscous stresses are fully dissipative. In the next section, the nonsymmetric viscosity will be applied to the 100:1 aspect ratio problem, which the symmetrized viscosity could not run.

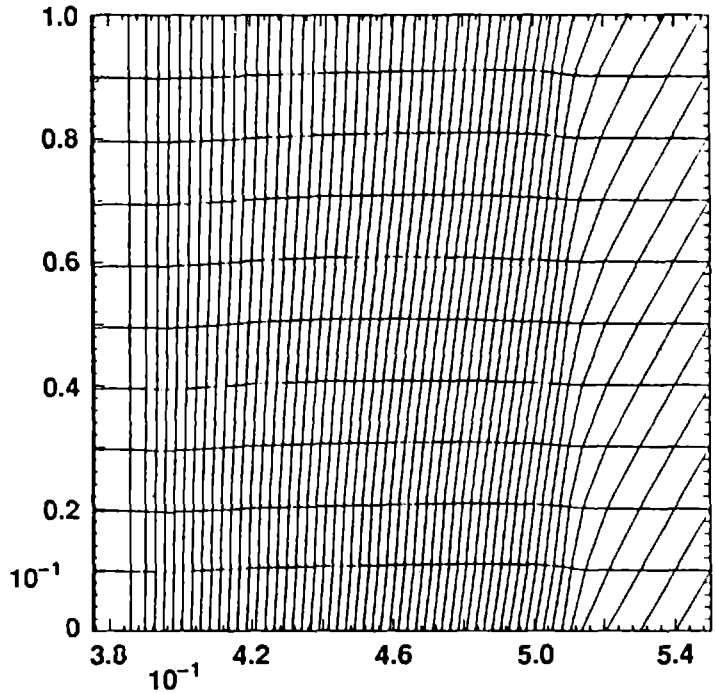

Figure 8. The nonsymmetric viscous stress tensor, coupled with extrapolated boundary conditions produce a result much like Fig. 4. Note the lack of a kink in the j-lines one cell in from the top and bottom boundaries.

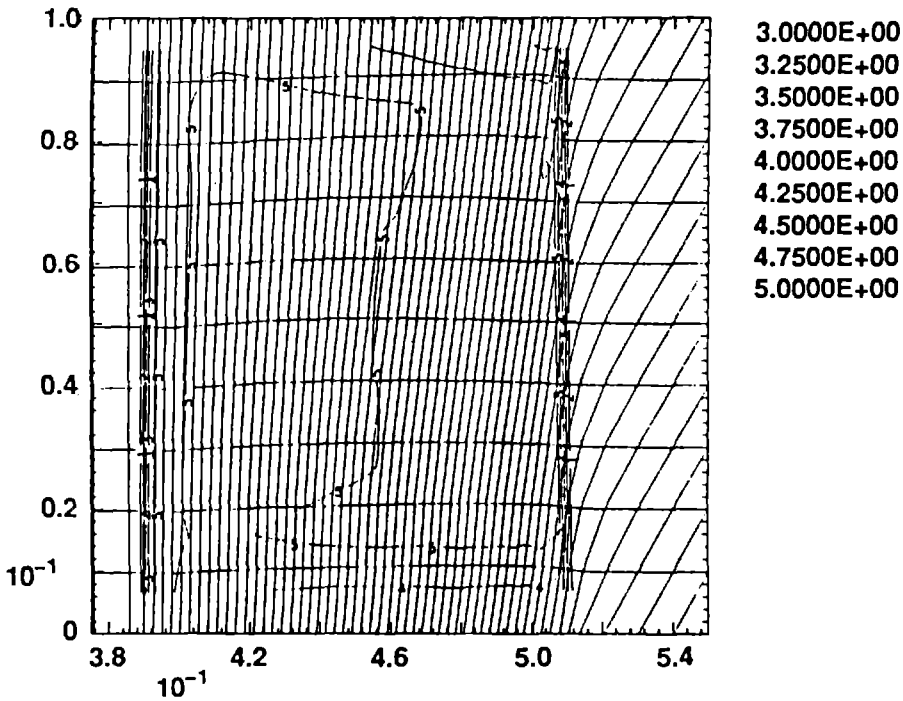

Figure 9. The density contours are overlaid on the mesh of Fig. 8.

V. Large Aspect Ratio Cells

The results of SHALE with the nonsymmetric viscosity tensor described in the previous section are shown in Figs. 10 and 11. The waviness present in the 1:1 aspect ratio problem is gone from the horizontal mesh lines. Presumably the transverse signals are generated by the main motion horizontally, and so are unchanged in magnitude. However, they must act over a much longer distance and so become negligible.

The artificial viscosity as formulated to this point does have some difficulty on the axis. The mesh and the density contours clearly show that a jet has formed, breaking the plane symmetry that is expected. Furthermore, the nodes on the axis have begun to pile up, and it their closeness that is controlling the timestep. Because the problem shows up on the boundaries and the interior of the mesh looks quite good, it might appear that there was some error in the boundary conditions. However, this is not the case.

To understand the problem, one should look for the differences between the calculation on the standard mesh and on the stretched mesh. It is clear that most of the material motion is in the y-direction—i.e., along the axis of the cylinder or equivalently along the i-edges as the problem is zoned. Now the relative accelerations along the k-edges are the same in both calculations. This is because the relative forces increase like the area of the j-edges (that is, like $|\mathbf{n}|$), and so do the masses of the vertices. On the other hand, the relative accelerations along the j-edges are much smaller in the stretched than in the standard problem, for the forces go like the area of the i-edges (like $|\mathbf{m}|$) which does not change while the mass increases. The principal $\Delta\mathbf{u}$ along the j-edges is mainly perpendicular to these edges, and so is seen as a shear. The resultant forces are important, and their almost total absence in the stretched problem leads to the axis jet.

It is easy to verify that this is the problem. If I assume that there is something special about the 1:1 mesh (supported by the experimental evidence that the numerical flow on the 1:1 mesh is better than on any other mesh), then I should simply scale the coefficient C^2 by the ratio of the areas ($|\mathbf{l}|/|\mathbf{k}|$) within each cell. I did this and it mostly eliminated the jet. However, it is not clear what is special about the 1:1 mesh. Instead I developed the following argument, which leads to a somewhat different, yet effective fix.

Beginning with Eq. (7), the relative acceleration of vertex 2 with respect to vertex 1 can be written

$$\frac{d(\Delta v)}{dt} = \frac{dv_2}{dt} - \frac{dv_1}{dt} = -\frac{1}{M} q_{\alpha\beta} n_\beta$$

Here I have assumed that the vertex mass associated with vertex 1 (M_1) and vertex 2 (M_2) are approximately equal, say to M. Now substitute for $q_{\alpha\beta}$ from Eqs. (13) and (17):

$$\frac{d(\Delta v)}{dt} = \frac{\rho\,[c_1 c_s + c_q\,|\,\Delta v\,|]\,|\,\mathbf{k}\cdot\mathbf{n}\,|\,\Delta v}{M\,|\,\mathbf{k}\,|} \tag{20}$$

Finally, approximate $\rho\,|\,\mathbf{k}\cdot\mathbf{n}\,| \sim M$. Then Eq. (20) can be written

$$\frac{1}{\Delta v}\,\frac{d(\Delta v)}{dt} = \frac{[c_1 c_s + c_q\,|\,\Delta v\,|]}{|\,\mathbf{k}\,|} \tag{21}$$

Assume that the right-hand side of Eq. (21) can be treated as constant during a computational timestep dt and integrate over the timestep:

$$\frac{|\,\Delta v\,(t+\delta t)\,|}{|\,\Delta v\,(t)\,|} = \exp(-C) \tag{22}$$

where C is a Courant number

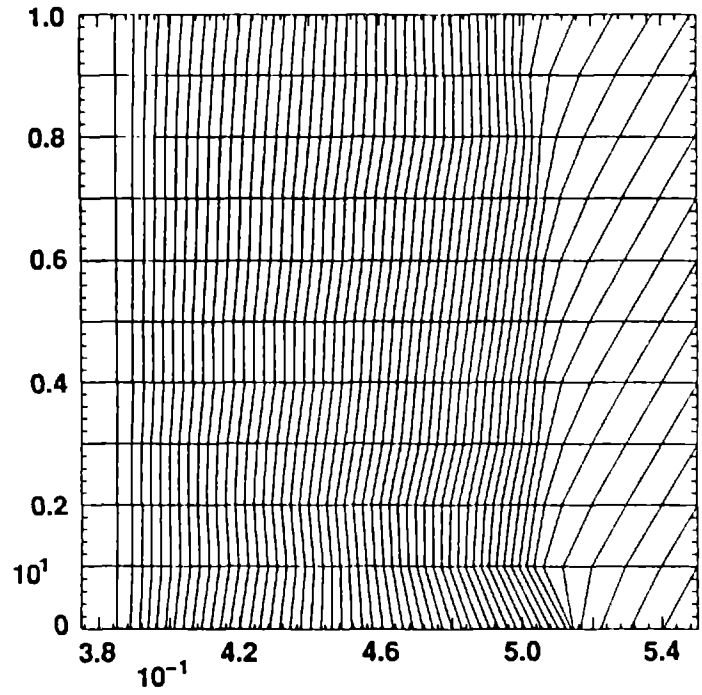

Figure 10. The 100:1 aspect ratio, run with the nonsymmetric tensor viscosity, shows a jet on the lower free slip boundary.

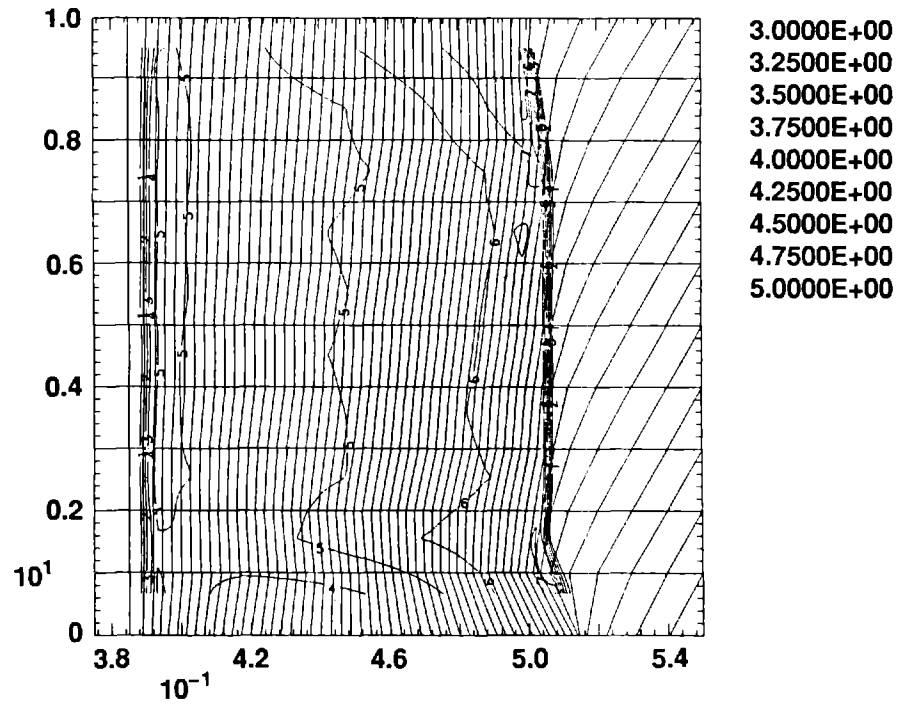

Figure 11. The same calculation of Fig. 10 with contours of density overlaid.

$$C = \frac{[c_1 c_s + c_q \mid \Delta v \mid]}{\mid k \mid} \delta t \tag{23}$$

The Courant number of a cell is a dimensionless number which, among other things, controls the timestep of the calculation. In SHALE, as well as in most explicit codes, a critical value of C is built into the code. In SHALE this critical value is 0.25, and in any case it must be less than 1. In every cell and in every cycle a value of the timestep is found that ensures the local Courant number is less than the critical value. The minimal value of the timestep over the mesh is the timestep for the entire mesh in the next cycle. When the Courant number is chosen to be 0.25, this means that a shock requires approximately four timesteps to traverse a cell.

Now Eq. (22) is an interesting result, for with the choices of the dimensionless numbers $c_1 = 1$ and $c_q = 1$, the effect of the artificial viscosity scales exactly with Courant number that SHALE uses to calculate the timestep. This is no accident. If I change the form of the Courant number that determines the timestep, then the optimal choice of the dimensionless coefficients (as determined by experiment) also changes. Equation (22) says that the (dimensionless) rate of damping of relative velocity depends only on the dimensionless Courant number.

The cell has two Courant numbers, one associated with the side k (C_k) and one with the side l (C_l). It is C_k that appears in Eq. (22). If I had started with Δv for vertices 2 and 3, then C_l would have resulted. C_l determines the rate at which relative velocity is damped along the cell side l. But if the shock is crossing the cell mainly along the direction k and C_k is controlling the timestep, then $C_l < C_k$ and the damping of the relative velocity along the side l will be too small. This is exactly what is happening in the piston problem with the 100:1 aspect ratio and leads to the jet.

The arguments above suggest that the scaling of the two viscous coefficients should depend on the Courant numbers of the two sides rather than on their areas. To summarize, define the Courant numbers

$$C_k = \frac{[c_1 c_s + c_q \mid A \mid]}{\mid k \mid}$$

$$C_l = \frac{[c_1 c_s + c_q \mid B \mid]}{\mid l \mid} \tag{24}$$

Then define the two viscous coefficients by

$$C^1 = \rho \mid k \mid \max\left(\frac{C_k}{\mid k \mid}, \frac{C_l}{\mid l \mid}\right)$$

$$C^2 = \rho \mid l \mid \max\left(\frac{C_k}{\mid k \mid}, \frac{C_l}{\mid l \mid}\right) \tag{25}$$

When the coefficients of viscosity are rescaled according to Eq. (25) and the calculation of the 100:1 piston problem repeated, the calculations shown in Figs. 12 and 13 result. These are a substantial improvement over the results of Figs. 10 and 11. The jet is gone, replaced by a slight tendency to lag on the axis. The mesh is smooth and the region behind shock is free of contour lines indicating that the density variations in this region are less than 7%. The average timestep is significantly higher and in fact is comparable to that found in the 1:1 piston problem.

The lagging of the flow on the bottom horizontal boundary is due to the hourglassing of the cells. The continuous change in slope of the j-lines causes each cell to each have a small hourglass deformation. The hourglassing slightly changes the effect of the ghost cells on the boundary.

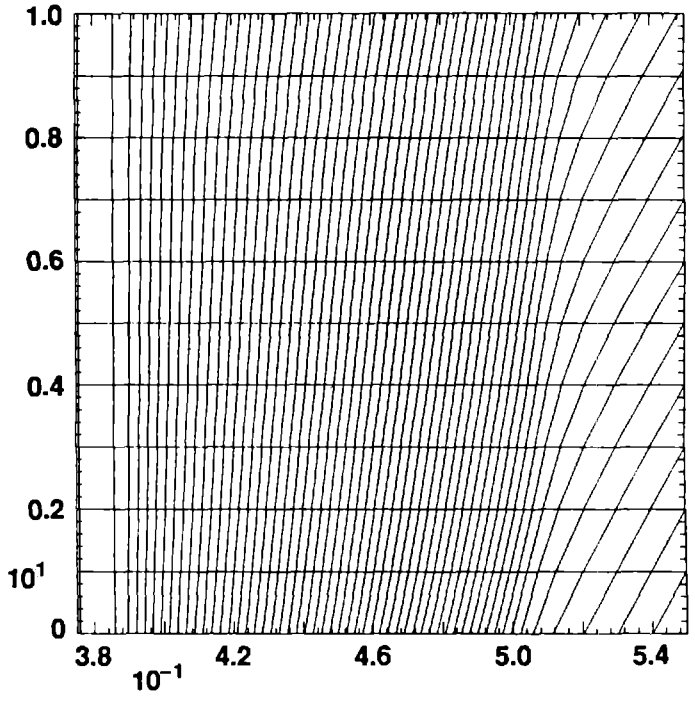

Figure 12. The 100:1 piston problem run with the nonsymmetric viscous tensor and Courant scaling of the viscous coefficient.

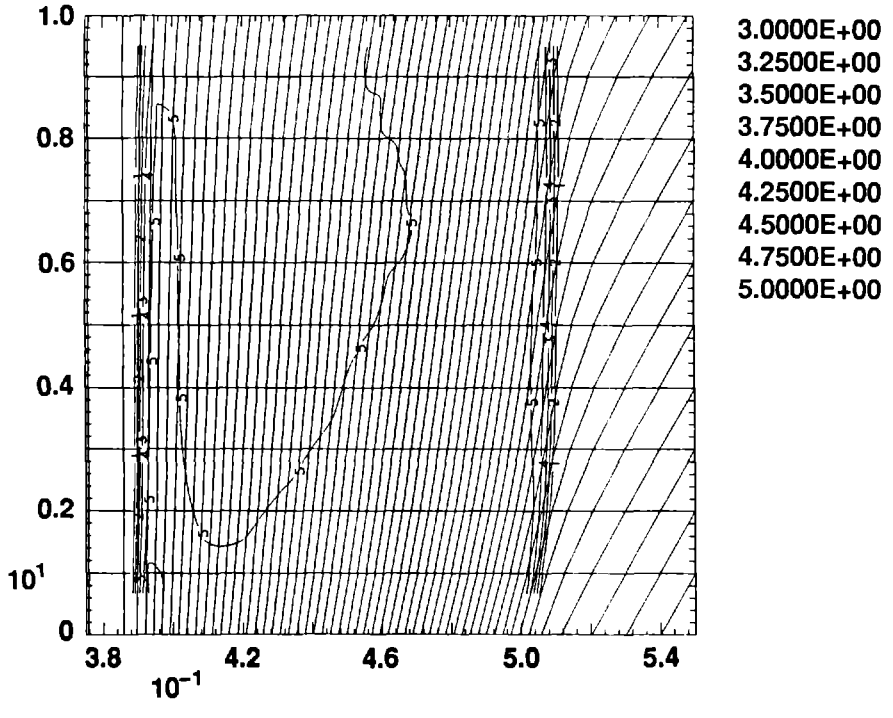

Figure 13. The same calculation as Fig. 12 with density contours overlaid.

VI. Cylindrical Symmetry

So far, the development has implicitly assumed that a Cartesian space. In generalizing the arguments there are two ideas to preserve. First, the viscosity should be a tensor—i.e., it should be constructed out of other objects that are tensors. Second, it should produce the same relative accelerations that were described in Sec. II. (The arguments of Sec. IV can be interpreted to say that it is the relative accelerations and not the relative forces that are important in Schulz' formulation. To generalize Eq. (13) one must choose between divergence and gradient (these are the same in Cartesian coordinates.) The proper choice is the gradient operator. With this choice in cylindrical coordinates, an additional term appears in the stress tensor. This is the hoop stress component, or $q_{\theta\theta}$, and has the form

$$q_{\theta\theta} = \frac{u}{r}\left[C_1 \frac{|\,k_1\,|^2}{|\,k\,|} + C_2 \frac{|\,l_1\,|^2}{|\,l\,|} \right] \tag{26}$$

where k_1 and l_1 are the radial components of the vectors k and l.

The Saltzman piston problem does not provide a real test of the differences between Cartesian and cylindrical calculations since the radial component of velocity is always much smaller than the axial component. One difference worth noting is that the boundary conditions described in Sec. IV must be further modified when the cylindrical axis of symmetry is a free slip boundary. When the idea of extrapolated boundaries is implemented in cylindrical coordinates, I found it necessary to replace the axis of symmetry with a small cylinder of finite radius, find the net force on the boundary nodes as a function of that radius, and then take the limit as the radius goes to zero. The result is that the net accelerations double on the axis of symmetry.

VII. Summary

In this section I will summarize my new artificial viscosity. Assuming that the cell is an arbitrary quadrilateral, whose vertices are numbered counter-clockwise from 1 to 4, define two vectors whose components are

$$\begin{aligned} k &= 0.5\,(x_2 + x_3 - x_1 - x_4,\; y_2 + y_3 - y_1 - y_4) \\ l &= 0.5\,(x_3 + x_4 - x_1 - x_2,\; y_3 + y_4 - y_1 - y_2) \end{aligned} \tag{27}$$

Next, calculate the spatial gradient of the velocity field. The gradient is a two-index tensor, calculated at the cell center—$\partial u_\alpha / \partial x_\beta$.

The artificial viscous stress has the form

$$q_{\alpha\beta} = \rho\, C\, \frac{\partial u_\alpha}{\partial x_\gamma}\,(k_\gamma k_\beta + l_\gamma l_\beta) \tag{28}$$

where

$$C = \max\left(\frac{c_1 c_s + c_q \left|\, \frac{\partial u_\alpha}{\partial x_\gamma} k_\gamma \,\right|}{|\,k_\gamma\,|}, \frac{c_1 c_s + c_q \left|\, \frac{\partial u_\alpha}{\partial x_\gamma} l_\gamma \,\right|}{|\,l_\gamma\,|} \right) \tag{29}$$

In these equations, ρ is the cell density, c_s is the sound speed of the material in the cell, and c_1 and c_q are the (dimensionless) coefficients of artificial viscosity. They should be chosen to optimize the shape of the shock. The choice $c_1 = 1$ and $c_q = 1$ work well in SHALE.

Note that the viscous stress of Eq. (28) is not a symmetric tensor. This is appropriate if extrapolated velocity boundary conditions are used. If reflected velocity boundary conditions are used, the viscous stress should be symmetrized. This latter choice may not work well for large aspect ratio cells.

The viscous stress in Eq. (28) is calculated at the cell center, and so should be added to the pressure and/or physical stresses to compute the acceleration.

Acknowledgements

It is a pleasure to acknowledge the help of several people in developing these ideas. Pat Crowley spent many hours discussing results and making suggestions. Don Burton and Steve Hornstein worked hard to help me understand Schulz' work. John Bolstad first brought the Saltzman piston problem to my attention, and contributed the calculations in Appendix B.

Appendix A

The Saltzman Piston Problem

The Saltzman piston problem is a test of the ability of a numerical fluid code to maintain plane symmetry of a one-dimensional flow through a two-dimensional mesh. The physical problem is the steady compression of a gas in a box, one of whose ends is a movable piston. I shall refer to the box as a cylinder whether the problem is run in Cartesian or in cylindrical coordinates. The flow in the cylinder is divided into two homogeneous regions. Furthest from the piston, the gas is still in its initial state. Immediately ahead of the piston, the gas is compressed and heated. The two regions are separated by a shock discontinuity. If the walls of the cylinder are perfectly smooth, the shock front is planar. The conservation laws of mass, energy and momentum plus the equation of state allow one to express the thermodynamic variables and the velocity of the shocked material in terms of those variables of the gas in the initial state, plus the piston velocity [13]. The initial conditions of the problem are shown in Table A-1.

The gas obeys a polytropic gas equation of state with $\gamma = 5/3$. The sound speed in the gas in its initial state is two orders of magnitude smaller than the piston velocity, and so the shock appears to be of infinite strength.

The problem is run in two spatial dimensions, and the mesh is constructed so that the shock front enters most of the cells obliquely—i.e., the shock front is not parallel to most of the cell edges in the problem. The numerical grid is oriented so that the piston moves along the y-axis. The mesh is 10 cells wide in the x-direction and 100 cells long in the y-direction. In logical space, the i-lines are straight and parallel to the x-axis. The j-lines begin parallel to the piston face, but gradually slant. Near the middle of the cylinder, the j-lines form a 45° angle to the y-axis. This is the maximum angle, and the slant then decreases.

Let W be the width and L be the length of the cylinder. The x- and y-coordinates of the nodes as a function of their logical coordinates i and j are given by

$$x(i, j) = (i-1) * dx$$

$$y(i, j) = (j-1) * dy + (i-1) * dy * \sin\theta \qquad \text{(A-1)}$$

where $dx = 0.1\,W$ and $dy = 0.01\,L$ and $\theta = \pi \dfrac{(j-1)}{100}$

and $i = 1,2,\ldots 11$ and $j = 1,2,\ldots..101$

Table A-1. Physical parameters for the Saltzman Piston Problem

piston velocity	10.0	cm/sec
material velocity	0.0	cm/sec
density	1.0	g/cm^3
internal energy	0.01	erg/g
cylinder length	1.0	cm
cylinder width	0.1	cm

The mesh is shown to scale in Fig. A-1.

In these units, the standard time for comparison of each of the runs in this paper (except for Sec. VII) is t = 0.375, when the shock is halfway down the mesh. Contours of density are always shown from 3. to 5. g/cm^3 in increments of 0.25 g/cm^3. The exact solution behind the shock is given below.

Table A-2. The exact solution behind the shock for the Saltzman piston problem.

pressure	133.3	dyn/cm^2
density	4.0	g/cm^3
internal energy	50.0	erg/g
shock velocity	13.3	cm/sec

The results of a calculation with the published version of SHALE are shown in Figs. A-2 through A-5. In these figures, and all the results shown in this paper, the vertical scale is stretched to make the results more easily visible.

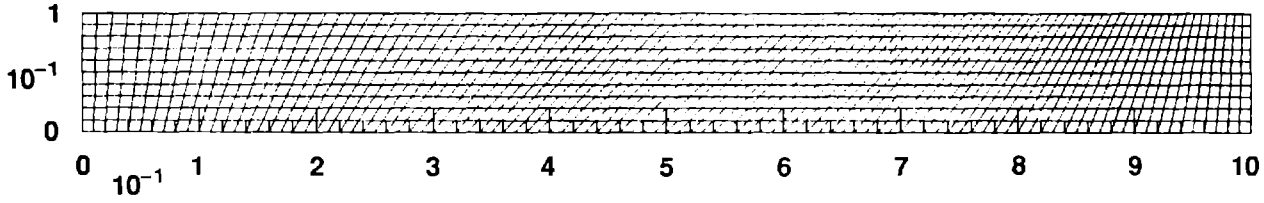

Figure A-1. The initial mesh for the Saltzman piston problem shown to scale and rotated so that the y-coordinate is horizontal. The piston pushes from the left with a constant specified velocity. The top, bottom, and right side are free slip.

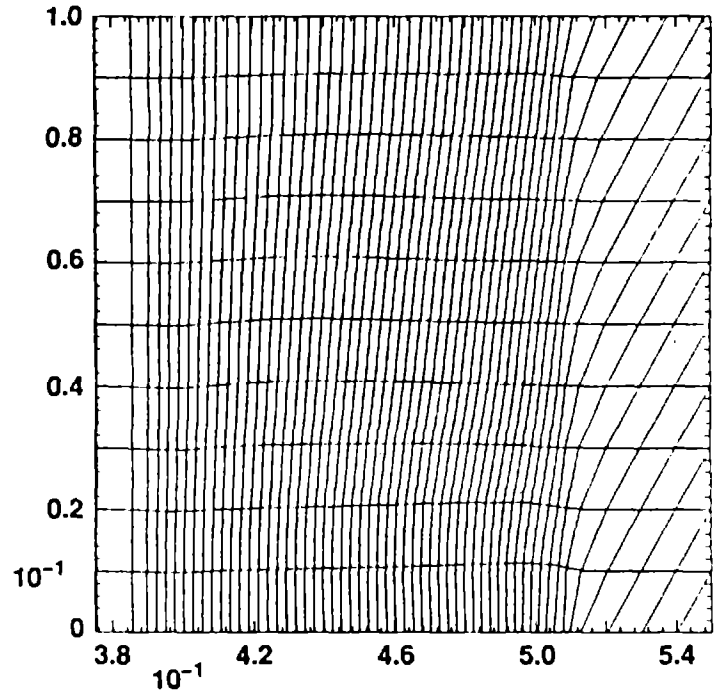

Figure A-2. The old viscous formulation in SHALE, run in fully tensor mode.

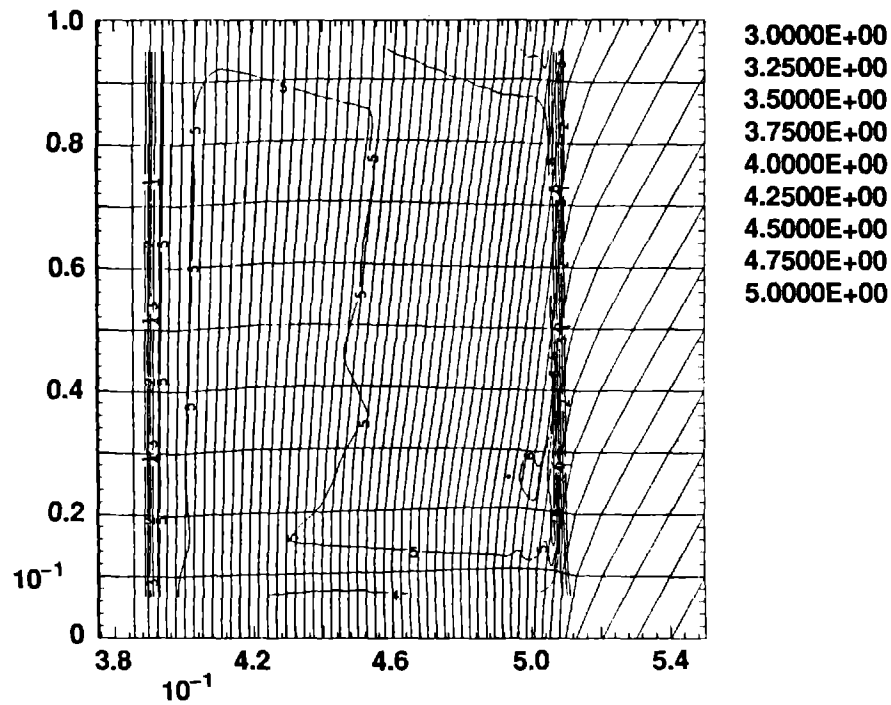

Figure A-3. The calculation of Fig. A-2 with contours of density overlaid.

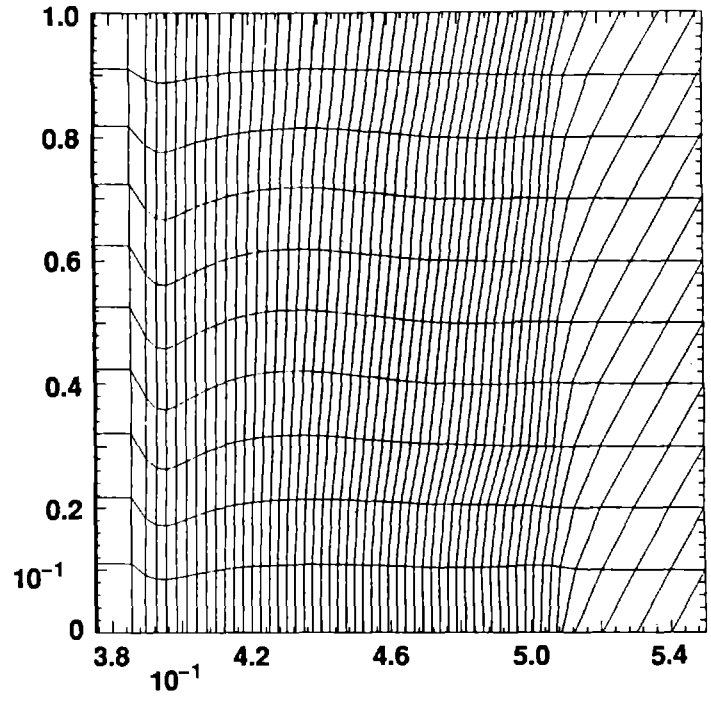

Figure A-4. The old viscous formulation in SHALE, run in fully scalar mode.

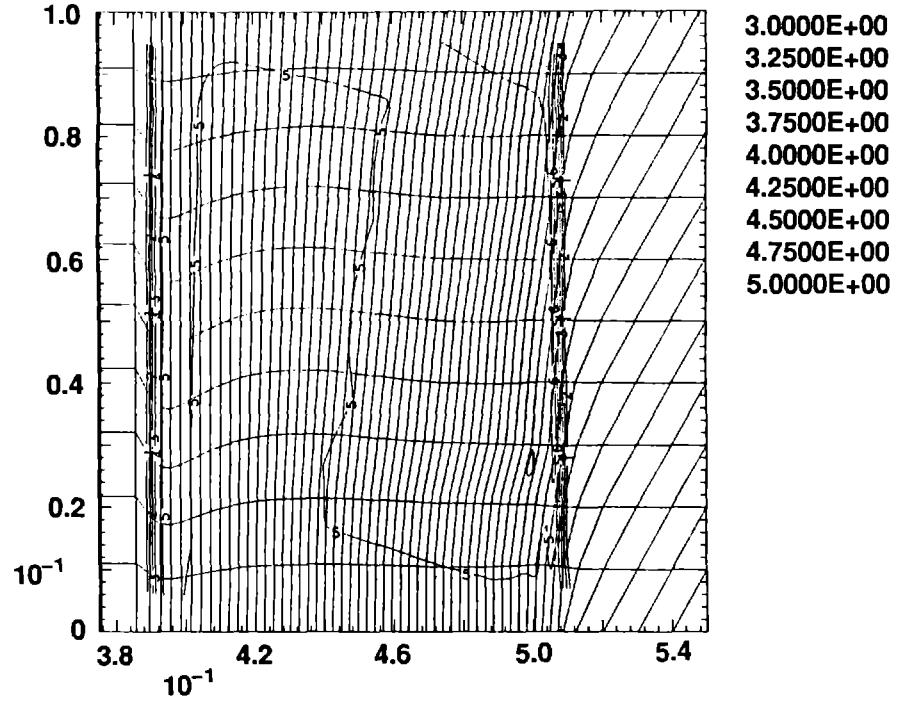

Figure A-5. The calculation as Fig. A-4 with contours of density overlaid.

Appendix B

The Barton Fix

In this appendix, I want to present some calculations made with the SIMPLE [14] code to illustrate an important, though unpublished, contribution to the use of edge-centered viscosity. Since none of this work is mine, let me begin by giving credit to Bob Barton. Barton is principally responsible for what is now called the "Barton Fix" to Schulz' viscosity. Credit for this development is shared with Jim Le Blanc and Jim Wilson. More recently, Bob Tipton and John Bolstad discovered the importance of Barton's fix in the context of shock propagation obliquely through a mesh, and in particular for the Saltzman piston problem. John Bolstad also supplied the calculations in this appendix.

SIMPLE [14] includes a straightforward implementation of the algorithms described by Schulz in a two-dimensional hydrodynamics code. In particular, the published version of the code contains the Schulz edge-centered viscosity in which the resultant force between nodes lies along the line joining them. When this version of SIMPLE is applied to the Saltzman piston problem, the mesh of Fig. B-1 and the density contours of Fig. B-2 result. SIMPLE has calculated a more or less plane shock at about the correct position. However, the contour plot shows considerable variation in the density behind the shock. The mesh plot shows very bad distortions, both at the piston face and along the axis of symmetry just behind the shock. This piling up of nodes will cause the problem to crash shortly after this time due to timestep controls.

The Barton fix consists of changing the direction of the resultant force between nodes, so that it lies along the direction of the relative velocity. The magnitude of the forces is unchanged. When only this change is made in SIMPLE and the problem is rerun, the results are dramatically improved. Figures B-3 and B-4 show the new mesh and density contours. The mesh is significantly better than Fig. 1. The contours show a more constant state of density behind the shock. The piling up of the nodes along the axis of symmetry is also gone, although the shock still shows a small jet in this region.

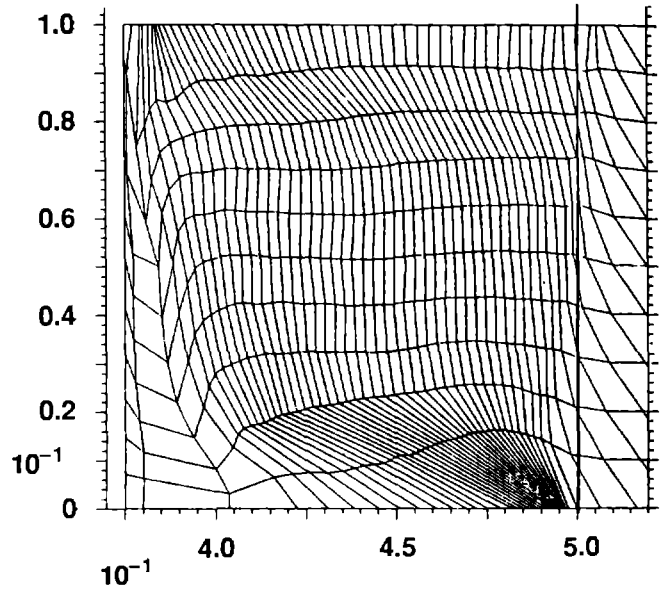

Figure B-1. The 1:1 piston problem, run on SIMPLE, without the Barton correction to the direction of the force.

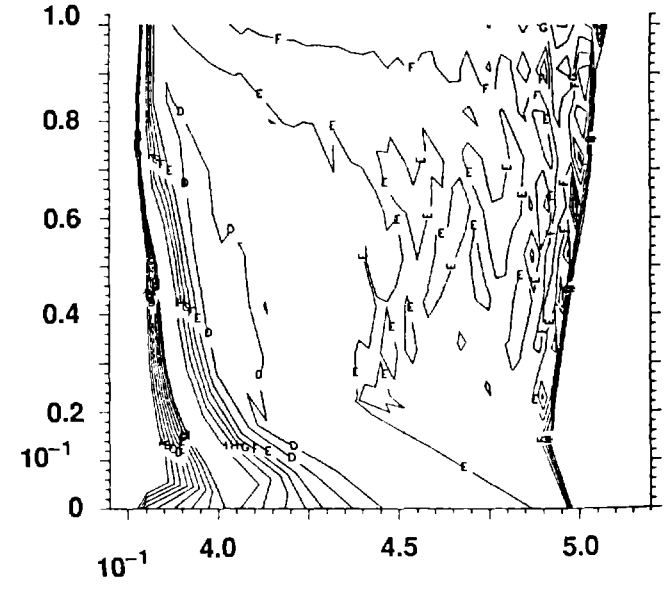

Figure B-2. The same calculation as Fig. B-1 with contours of density overlaid.

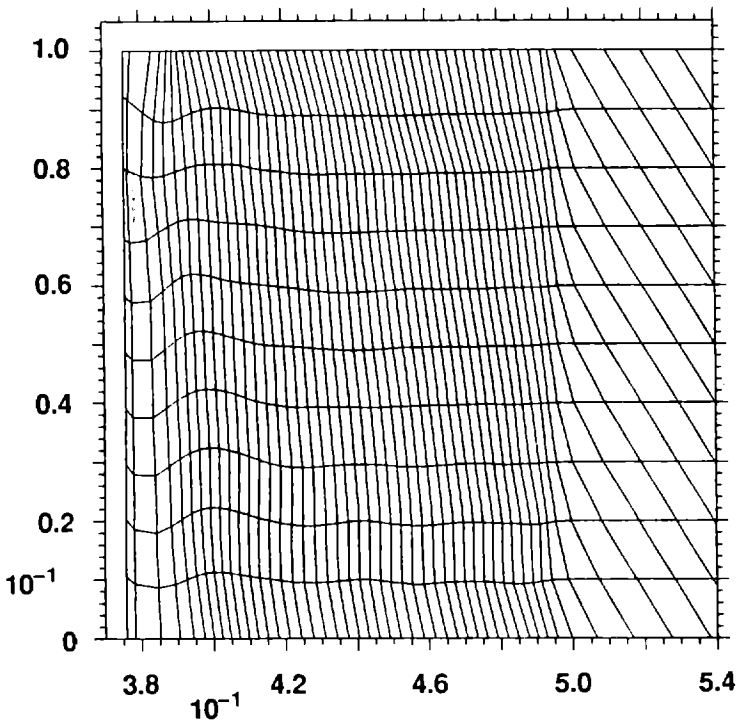

Figure B-3. The 1:1 piston problem, run on SIMPLE, with the Barton correction to the direction of the force.

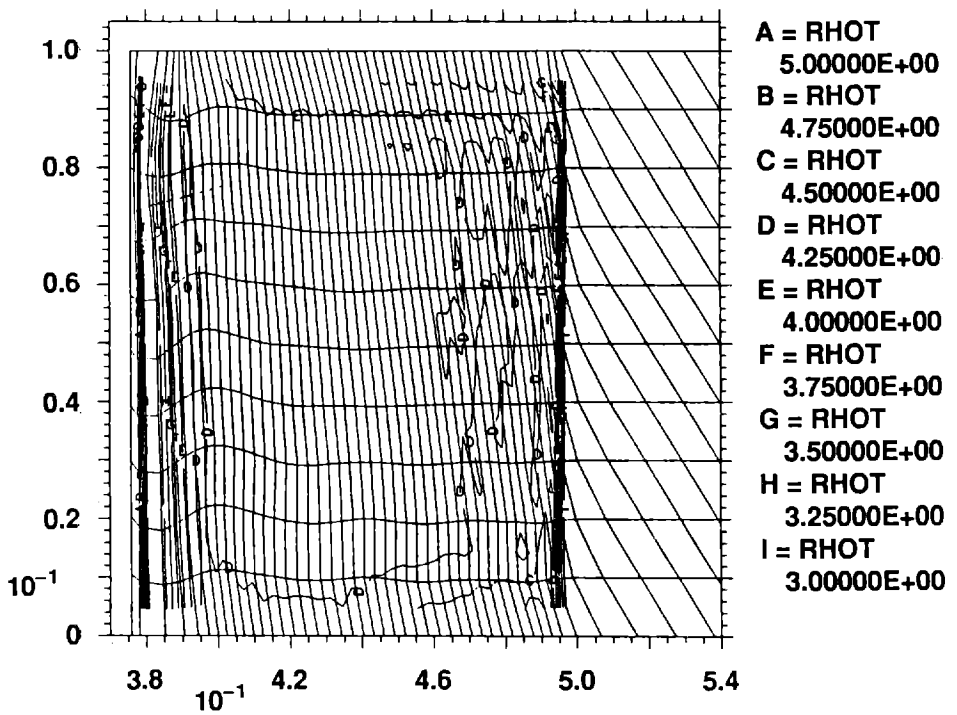

Figure B-4. The same calculation as Fig. B-3 with contours of density overlaid.

References

1. J. von Neumann and R. D. Richtmyer, *J. Appl. Phys.* **21**, p. 232 (1950).

2. M. L. Wilkins, *J. Comp. Phys.* **36**, p. 281 (1980).

3. R. B. Demuth, L. G. Margolin, B. D. Nichols, T. F. Adams and B. W. Smith, *SHALE: A Computer Program for Solid Dynamics*, Los Alamos National Laboratory Report LA 10236, May, 1985.

4. W. D. Schulz, "Two-Dimensional Lagrangian Hydrodynamic Difference Equations," in *Methods in Computational Physics*, Vol. 3, B. Alder, S. Fernbach and M. Rotenberg, Eds., Academic Press, p. 1 (1964).

5. S. K. Godunov, *Mat. Sb.* **47**, p. 271 (1959).

6. B. Van Leer, *J. Comp. Phys.* **32**, p. 101 (1979).

7. P. L. Roe, *J. Comp. Phys.* **43**, p. 357 (1981).

8. L. G. Margolin, H. M. Ruppel, and R. B. Demuth, *Gradient Scaling for Nonuniform Meshes*, Proc. the Fourth International Conference on Numerical Methods in Laminar and Turbulent Flow, Swansea, U. K., p. 1477 (1985).

9. W. F. Noh, *Errors for Calculations of Strong Shocks Using an Artificial Viscosity and an Artificial Heat Flux*, Lawrence Livermore National Laboratory Report UCRL-53669 (1985).

10. P. Colella and J. Saltzman, submitted to *J. Comp. Phys.*

11. L. G. Margolin and J. J. Pyun, *A Method for Treating Hourglass Patterns*, Proc. the Fifth International Conference on Numerical Methods in Laminar and Turbulent Flow, Montreal, Canada (1987).

12. L. G. Margolin and T. F. Adams, *Spatial Differencing for Finite Difference Codes*, Los Alamos National Laboratory Report LA 10249 (1985).

13. F. H. Harlow and A. A. Amsden, *Fluid Dynamics*, Los Alamos National Laboratory Report La-4700 (1971).

14. W. P. Crowley, C. P. Hendrickson and T. E. Rudy, Lawrence Livermore National Laboratory Report UCID-17715 (1978).